



OPEN Jaw1 accelerates the reaction speed of the Ca²⁺ signals via ITPRs upon GPCR stimulation

Takuma Kozono^{1,3}, Hitomi Matsui^{2,3}, Marielle Fernandez Bandalan², Takashi Tonzuka² & Atsushi Nishikawa²✉

Jaw1/LRMP/IRAG2 enhances Ca²⁺ release via interaction with inositol 1,4,5-trisphosphate receptors (ITPRs), Ca²⁺ channels on the endoplasmic reticulum, upon G protein-coupled receptor stimulation. While our previous works demonstrated the increases in the maximum amplitude and retention time of the Ca²⁺ curve with heterogeneous effects on each ITPR subtype: ITPR1, ITPR2, and ITPR3, the effects on the reaction speed remain unclear. In this study, we unveiled the additional roles of Jaw1 in accelerating the signal onset time and rise time to the first peak top, especially in the cells expressing ITPR1. These findings shed more light on the relationship between the expression pattern of Jaw1 and ITPRs, and the heterogeneous pattern of the Ca²⁺ dynamics, offering insights into their physiological implications.

Keywords Ca²⁺ signaling, Jaw1/IRAG2/LRMP, ITPRs

Ca²⁺ signals serve as pivotal regulators for various cellular processes such as cell proliferation, cell differentiation, gene transcription, secretion, fertilization, metabolism, etc.^{1,2}. The signal is often triggered by extrinsic stimuli. When the G protein-coupled receptors (GPCR) are stimulated, inositol 1,4,5-trisphosphate (IP₃) is produced by phospholipase C. IP₃ then binds to inositol 1,4,5-trisphosphate receptors (ITPRs), Ca²⁺ channels on the endoplasmic reticulum (ER), which evokes the Ca²⁺ release from the ER to the cytoplasm^{3,4}. The released cytoplasmic Ca²⁺ regulates effector proteins, leading to diverse downstream cellular responses that occur over different time scales, ranging from microseconds to hours^{5,6}.

The Ca²⁺ dynamics are spatially and temporally visualized by monitoring the fluorescence intensity of loaded Ca²⁺ binding dyes or genetically encoded Ca²⁺ indicators^{7–10}. The fluorescence intensity is often plotted by the time-lapse acquisition (hereafter called Ca²⁺ curve). The patterns of the Ca²⁺ curve upon GPCR stimulation vary in terms of the reaction speed, strength, retention time, frequency, etc., depending on the involved ligands, receptors, other signaling-related molecules, cell types, etc.^{1,11–14}. ITPRs function as hubs involving several interactors that modulate their activities, thereby regulating Ca²⁺ signals in various ways: immediately, augmentatively, restrainedly, continuously, or frequently¹⁵. Moreover, ITPRs have three subtypes—ITPR1, ITPR2, and ITPR3—with different IP₃ affinities and Ca²⁺ signal patterns^{13,16–18}. Thus, the combination of factors such as the expression patterns of ITPRs and their regulators, ligand-receptor kinetics, and even the cell state ultimately shapes the patterns of Ca²⁺ signals. In other words, a dedicated pattern of Ca²⁺ signal is demanded for the specialized physiological functions of each cell type. Considering that Ca²⁺ signal patterns impact the function of each effector and subsequently influence cellular processes, it is extremely crucial to understand how each ITPR interactor affects its activity and shapes Ca²⁺ signal patterns.

Jaw1, also known as lymphoid-restricted membrane protein (LRMP) and inositol 1,4,5-trisphosphate receptor associated 2 (IRAG2), is a type II integral membrane protein localized at the ER and outer nuclear membrane. Our previous studies have established the role of Jaw1 in maintaining the nucleus and Golgi morphology in mouse melanoma B16F10 cells^{19,20}. Furthermore, we and other groups recently reported that Jaw1 interacts with ITPRs via its coiled-coil domain and enhances their Ca²⁺ release activities upon GPCR stimulation^{13,21,22}. Importantly, the expression of Jaw1 mutant lacking coiled-coil domain, a domain for interaction with ITPRs, canceled the augmentative effects of Jaw1 on the Ca²⁺ signals, which indicates that Jaw1 directly affects the functions of ITPRs. In our previous report, we demonstrated that the expression of Jaw1 causes the Ca²⁺ curve to have higher amplitude and more frequent oscillations (the phenomenon that the peaks occurred repeatedly on the Ca²⁺

¹Smart-Core-Facility Promotion Organization, Tokyo University of Agriculture and Technology, 3-5-8 Saiwai-cho, Fuchu, Tokyo 183-8509, Japan. ²Department of Applied Biological Science, Tokyo University of Agriculture and Technology, 3-5-8 Saiwai-cho, Fuchu, Tokyo 183-8509, Japan. ³Takuma Kozono and Hitomi Matsui contributed equally to this work. ✉email: nishikaw@cc.tuat.ac.jp

curve), but its effect on the reaction speed remains unknown. This report herein shows that Jaw1 accelerates the reaction speed of the Ca^{2+} signals, especially in the cells expressing ITPR1, using a more time-resolved Ca^{2+} assay. These findings will contribute to a deeper understanding for the roles of Jaw1 on the Ca^{2+} signals as well as the relationship between the Ca^{2+} dynamics via ITPRs and their modulation for the physiological systems.

Results

Jaw1 accelerates the reaction speed of the Ca^{2+} signals upon GPCR stimulation

The time scale of Ca^{2+} signal-related physiological responses is different on a range from microseconds to hours⁶. The quicker response can be detected by more time-resolved analysis. To evaluate the effect of Jaw1 on the reaction speed of the Ca^{2+} signals, we performed the time-lapse calcium assay at time intervals (0.11–0.13 s) as short as possible in our well-scanning plate reader, compared to those employed in our previous study (2 s)¹³. Based on the generated Ca^{2+} curves, the following factors: $\Delta T_{\text{stimulation-F1.2}}$, $\Delta T_{\text{stimulation-Fmax}}$, and $\Delta F/\Delta T_{\text{F1.2-F90\%}}$ as well as F_{max} and area under the curve (AUC), were calculated to investigate the signal onset time, rise time to the first peak top, rise rate, maximum amplitude, and retention time, respectively (see the section of “Materials and methods” for the details) (Fig. 1). For the assay, the following validated cell lines were used: HEK293 Flp-In T-REx cells lacking Jaw1 (Jaw1 KO) generated by CRISPR/Cas9-mediated genome editing technology and Jaw1 KO HEK293 Flp-In T-REx cells with doxycycline (Dox)-inducible expression of the exogenously introduced *Jaw1* gene (Jaw1 IE). The loss of Jaw1 in Jaw1 KO cells and inducible expression of Jaw1 in Jaw1 IE cells were confirmed by western blotting¹³. The protein expression levels of ITPRs were not altered between them¹³. In this context, the cells were loaded with Fluo-4, and the fluorescence intensities were recorded following GPCR stimulation with 1, 10, and 100 μM adenosine triphosphate (ATP). The F_{max} and AUC in Jaw1 IE cells were significantly higher than those in Jaw1 KO cells at each indicated concentration of ATP (Fig. 2A–C, G, H), consistent with our previous report¹³. Importantly, $\Delta T_{\text{stimulation-F1.2}}$ in Jaw1 IE cells was significantly shorter than that in Jaw1 KO cells at each indicated concentration of ATP (Fig. 2D–F, I). Furthermore, $\Delta T_{\text{stimulation-Fmax}}$ in Jaw1 IE cells was significantly shorter than that in Jaw1 KO cells at each indicated concentration of ATP (Fig. 2D–F, J). Of note, the mean differences in $\Delta T_{\text{stimulation-F1.2}}$ (on average: 1 μM ATP, 2.62 s; 10 μM ATP, 0.42 s; 100 μM ATP, 0.35 s) and $\Delta T_{\text{stimulation-Fmax}}$ (on average: 1 μM ATP, 6.04 s; 10 μM ATP, 2.13 s; 100 μM ATP, 1.50 s) between Jaw1 KO and Jaw1 IE cells were much more distinguished at lower concentrations of ATP, in contrast to that in AUC (Fig. 2H–J). $\Delta F/\Delta T_{\text{F1.2-F90\%}}$ in Jaw1 IE cells was significantly higher than that in Jaw1 KO cells at each indicated concentration of ATP (Fig. 2D–F, K). In summary, these results indicate that the expression of Jaw1 accelerates the signal onset time, rise time to the first peak top, and rise rate of the Ca^{2+} signals via ITPRs.

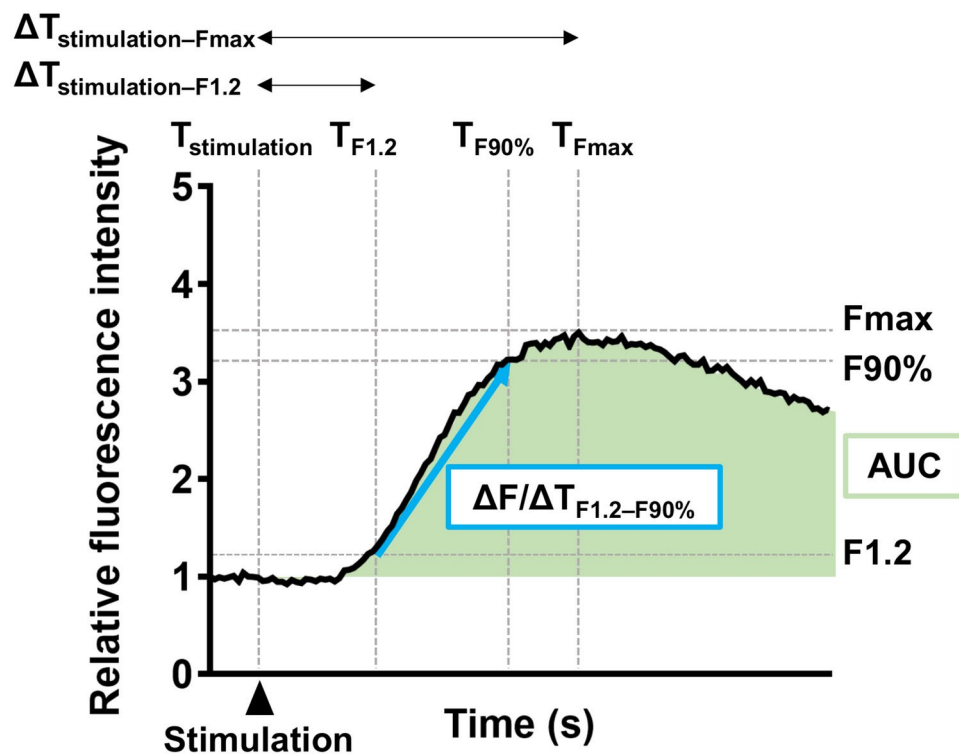


Fig. 1. The factors calculated from the Ca^{2+} curve in this study. $\Delta T_{\text{stimulation-F1.2}}$, $\Delta T_{\text{stimulation-Fmax}}$, and $\Delta F/\Delta T_{\text{F1.2-F90\%}}$ as well as F_{max} and area under the curve (AUC) are calculated based on the Ca^{2+} curve. (see the section of “Materials and methods” for the details).

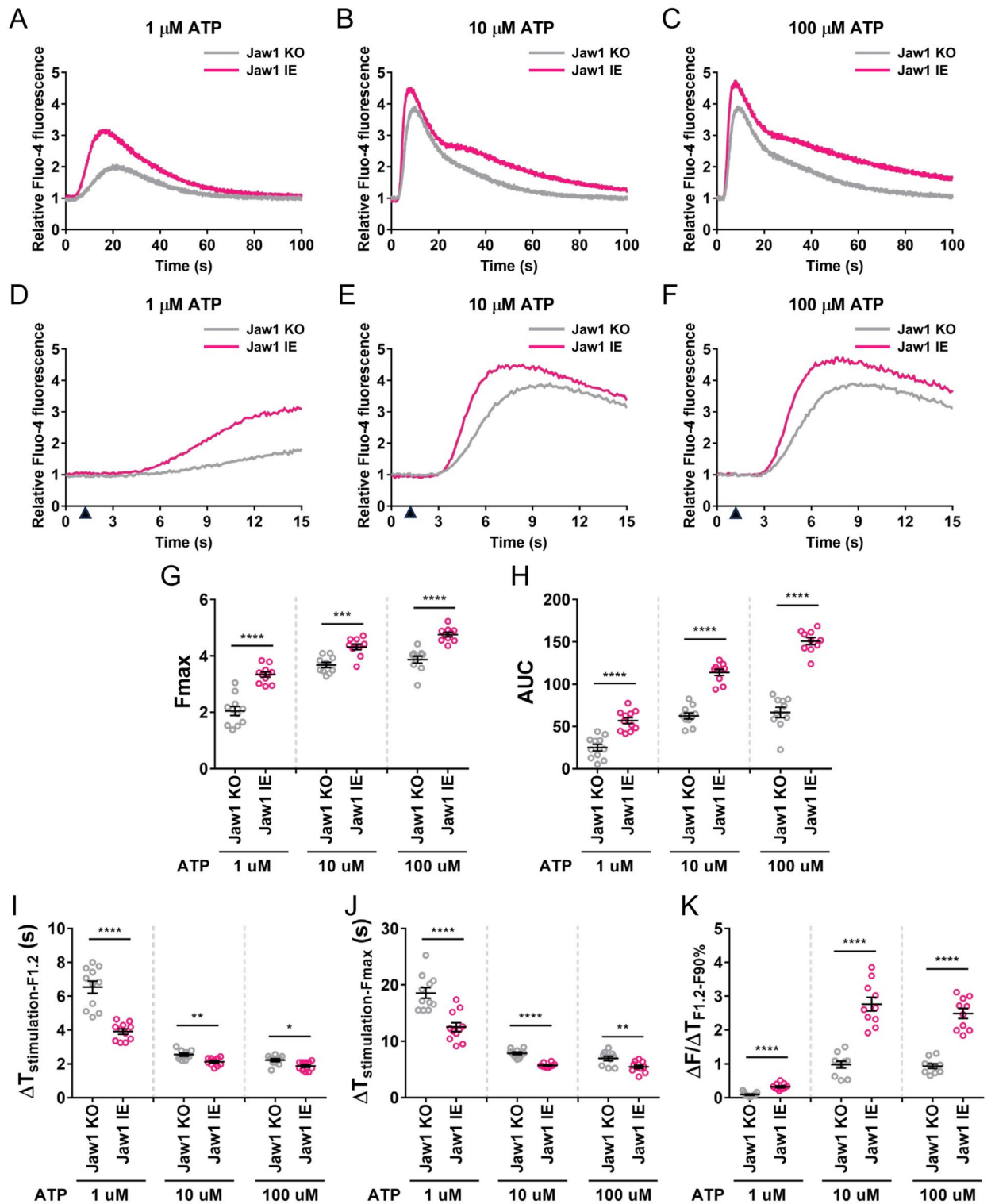


Fig. 2. Jaw1 accelerates the reaction speed of the Ca^{2+} signals upon GPCR stimulation. (A–C) Mean curves (0–100 s) of relative Fluo-4 fluorescence intensity upon stimulation with 1 (A), 10 (B), and 100 (C) μM ATP in Jaw1 KO and Jaw1 IE cells. The averages of three wells are plotted in the graphs. (D–F) Mean curves (0–15 s) are enlarged from (A), (B), and (C), respectively. Closed triangles represent the time points that ATP solution was added. (G–K) F_{max} (G), AUC (H), $\Delta T_{\text{stimulation-F1.2}}$ (I), $\Delta T_{\text{stimulation-Fmax}}$ (J), and $\Delta F/\Delta T_{\text{F1.2-F90\%}}$ (K) calculated from the plots in (A), (B), and (C). The averages of three independent experiments per condition ($n=3$ or 4) are shown in the graphs. In total, $n=11$. The error bar shows \pm S.D.; *, $p < 0.05$; **, $p < 0.01$; ***, $p < 0.001$; ****, $p < 0.0001$; statistical analysis, two-tailed Student's t -test.

Jaw1 accelerates the reaction speed of the Ca²⁺ signals in the cells expressing ITPR1

ITPRs have functional differences among subtypes, and the augmentative effects of Jaw1 are also different depending on the ITPR subtype^{13,16,18}. Here, we investigated the heterogeneous effects of Jaw1 on the reaction speed of the Ca²⁺ signals via each ITPR subtype by time-lapse calcium assay. For the assay, we first prepared Jaw1 KO HEK293 Flp-In T-REx cell lines exclusively expressing a single ITPR subtype: ITPR1, ITPR2, and ITPR3 (hereafter referred to as R1 SE, R2 SE, and R3 SE cells, respectively), which was validated in our previous report¹³. Subsequently, the *Jaw1* gene was exogenously introduced into the above-mentioned cells, and its expression was induced by the addition of Dox (hereafter referred to as R1 SE Jaw1 IE, R2 SE Jaw1 IE, and R3 SE Jaw1 IE). The inducible expression of Jaw1 in R1 SE Jaw1 IE, R2 SE Jaw1 IE, and R3 SE Jaw1 IE cell was confirmed by western blotting¹³. The protein expression levels of each ITPR were not altered between each cell line with and without Jaw1¹³. In this context, Fluo-4 loaded cells—with or without inducible expression of Jaw1—were stimulated with 1 and 100 μM ATP, and the Ca²⁺ curves of each cell line were compared (Fig. 3). The F_{max} and AUC in R1 SE Jaw1 IE and R2 SE Jaw1 IE cells were significantly higher than those in R1 SE and R2 SE cells, respectively, when the cells were stimulated at 1 μM ATP (Figs. 3A, B and 4A, B, D, E). This trend was the same when the cells were stimulated at 100 μM ATP (Figs. 3G, H and 4A, B, D, E). The F_{max} and AUC in R3 SE Jaw1 IE were slightly higher than those in R3 SE cells when stimulated with 100 μM ATP, while both R3 SE cells and R3 SE Jaw1 IE cells almost did not respond to the stimulation at 1 μM ATP (Figs. 3C, I and 4C, F). Such trends were consistent with our previous report wherein the cells were stimulated at 100 μM ATP and measured by fluorescence microscopy¹³. Furthermore, the trends of responsiveness in R1, R2, and R3 SE cells are consistent with previous reports that the IP₃ sensitivity (IP₃-induced Ca²⁺ release) for each ITPR subtype is in the order of ITPR2 > ITPR1 > ITPR3, and the unresponsiveness to 1 μM ATP in R3 SE cells but not R1 and R2 SE cells is probably due to the lowest IP₃ sensitivity of ITPR3^{16,17}. Importantly, $\Delta T_{\text{stimulation-F}_{1.2}}$ in R1 SE Jaw1 IE cells was significantly shorter than that in R1 SE cells at each indicated concentration of ATP (Figs. 3D, J and 5A). On the other hand, $\Delta T_{\text{stimulation-F}_{1.2}}$ in both R2 SE Jaw1 IE and R3 SE Jaw1 IE cells were comparable with that in R2 SE and R3 SE cells, respectively, at each indicated concentration of ATP (Figs. 3E, F, K, L and 5B, C). Furthermore, $\Delta T_{\text{stimulation-F}_{\text{max}}}$ in R1 SE Jaw1 IE cells was significantly shorter than that in R1 SE cells at each indicated concentration of ATP (Figs. 3D, J and 5D). On the other hand, $\Delta T_{\text{stimulation-F}_{\text{max}}}$ in both R2 SE Jaw1 IE and R3 SE Jaw1 IE cells were almost comparable with that in R2 SE and R3 SE cells, respectively, at each indicated concentration of ATP (Figs. 3E, F, K, L and 5E, F). $\Delta F/\Delta T_{\text{F}_{1.2}-\text{F}_{90\%}}$ in R1 SE Jaw1 IE cells, R2 SE Jaw1 IE cells, and R3 SE Jaw1 IE cells was significantly higher than that in R1 SE cells, R2 SE cells, and R3 SE cells, respectively, when the cells were stimulated at 100 μM ATP, and a significant difference was observed only between R1 SE Jaw1 IE and R1 SE cells when the cells were stimulated at 1 μM ATP (Figs. 3D–F, J–L and 5G–I). In summary, these results indicate that the expression of Jaw1 accelerates the signal onset time and rise time to the first peak top of the Ca²⁺ signals, especially in the cells exclusively expressing ITPR1, and augments the rise rate of the Ca²⁺ signals via all ITPR subtypes.

Discussion

Our previous work demonstrated that Jaw1 enhances the Ca²⁺ release activity of ITPRs upon GPCR stimulation, particularly in terms of the maximum amplitude and retention time^{13,22}. Importantly, these effects vary depending on the ITPR subtype. In our current study, we unveiled an additional accelerating effect of Jaw1 on the reaction speed of the Ca²⁺ signals. Specifically, this accelerating effect on the reaction speed was notable in cells exclusively expressing ITPR1, rather than those of ITPR2 or ITPR3.

For the patterning of the Ca²⁺ signals, the spatiotemporal localization at the ER of the functional ITPRs is crucial^{23,24}. Both IP₃ and Ca²⁺ are necessary to evoke Ca²⁺ release from ITPRs through processes known as IP₃-induced Ca²⁺ release (IICR) and Ca²⁺-induced Ca²⁺ release (CICR), respectively^{25,26}. Ca²⁺ blips, which are minimum Ca²⁺ release events from individual ITPRs, trigger adjacent ITPRs to open, leading to the occurrence of Ca²⁺ puffs—localized Ca²⁺ release events evoked from the clusters of ITPRs^{18,24,25}. These regenerative Ca²⁺ puffs, followed by Ca²⁺ diffusion, progressively amplify Ca²⁺ release from ITPRs based on the mechanism of the CICR across the entire cell. Ultimately, this process shapes the propagation of global Ca²⁺ waves throughout the cell^{18,24}. Particularly, the stimulation at higher concentrations of agonists spatiotemporally promotes the occurrence of the Ca²⁺ puff and CICR in the cells, accelerating the rise rate of the global Ca²⁺ wave²⁴. Interestingly, we previously reported that Jaw1 oligomerizes and interacts with ITPRs via the coiled-coil domain^{13,27}. Thus, we provide a hypothesis that the oligomerization of Jaw1 functions as a scaffold for the ITPR cluster, which promotes the formation of a larger ITPR cluster. This mechanism might increase the strength and probability of Ca²⁺ puff occurrences and ultimately accelerate the reaction speed of the global Ca²⁺ wave. Therefore, it will be our next task to investigate whether the expression of Jaw1 affects the formation of ITPR clusters and Ca²⁺ puffs through light microscopic analysis. Furthermore, the structural analysis by a cryo-electron microscope will be a key to understanding how Jaw1 oligomerizes and interacts with ITPRs.

To date, the activity of each ITPR has been investigated in several aspects such as strength, frequency, etc.^{16,18}. To our knowledge, this is the first comparative study to have investigated the reaction speed of Ca²⁺ signals in the cells exclusively expressing single ITPR subtypes. Interestingly, the reaction speed of the Ca²⁺ signals upon stimulation with ATP was fastest in cells expressing the ITPR subtypes in the order of ITPR2 > ITPR1 > ITPR3, as shown in Fig. 5. This trend is consistent with previous reports that the IP₃ sensitivity (IP₃-induced Ca²⁺ release) for each ITPR subtype is in the order of ITPR2 > ITPR1 > ITPR3^{16,17}. Nevertheless, the expression of Jaw1 accelerates the reaction speed of Ca²⁺ signals in the cells expressing ITPR1, rather than ITPR2 or ITPR3. It has been reported that the dependence of IP₃-induced Ca²⁺ release on Ca²⁺ concentration is higher in cells expressing the ITPR subtypes in the order of ITPR1 > ITPR2 > ITPR3¹⁶. In other words, ITPR1 might be more sensitive to the higher local Ca²⁺ concentration generated from the Ca²⁺ puff. Considering our hypothesis above, the strong and high probability of the Ca²⁺ puff occurrences due to the expression of Jaw1 might contribute to

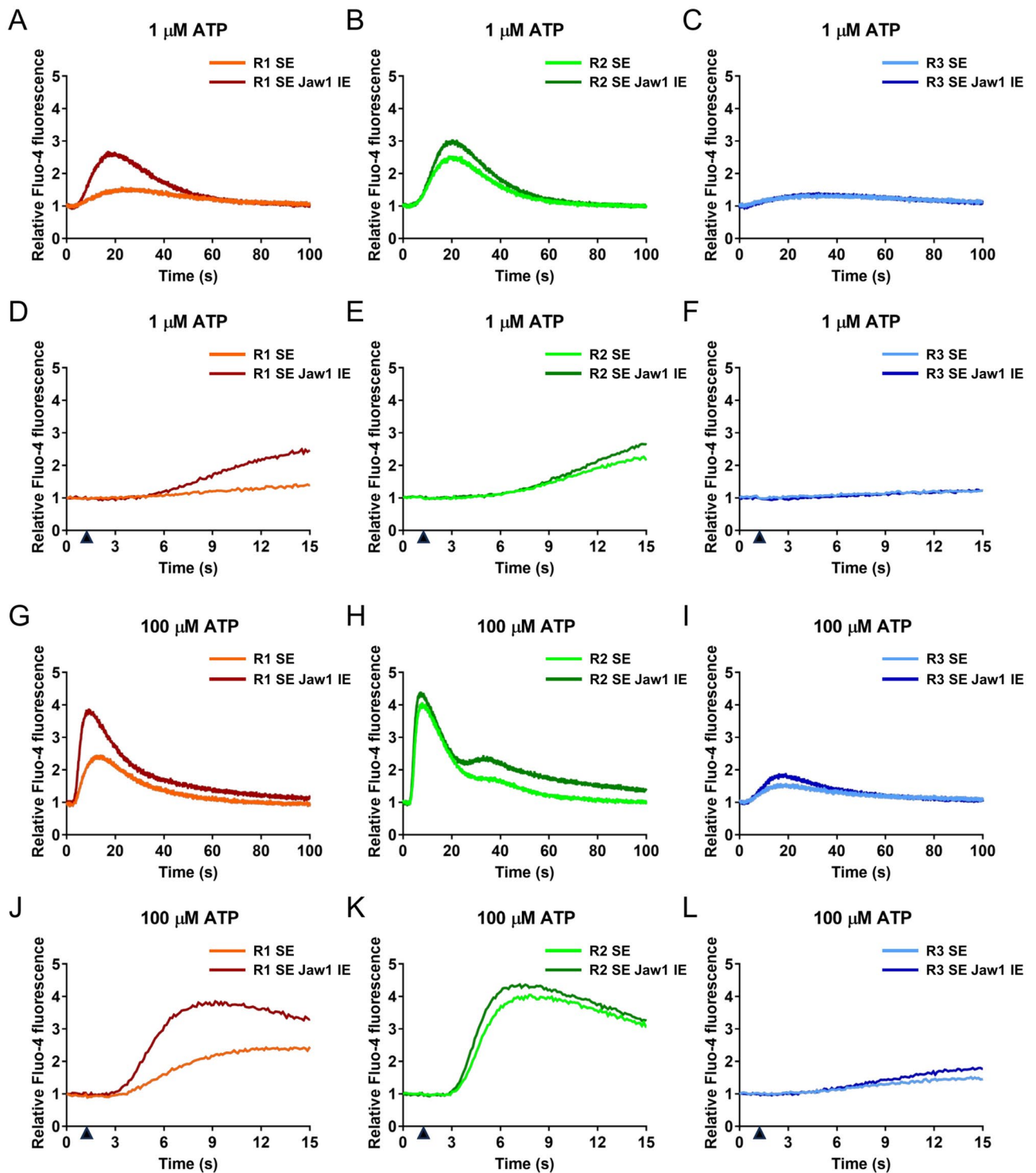


Fig. 3. Jaw1 increases the Ca^{2+} signals upon GPCR stimulation in the cells expressing all ITPR subtypes. (A–C and G–I) Mean curves (0–100 s) of relative Fluo-4 fluorescence intensity upon stimulation with 1 μM ATP (A–C) and 100 μM ATP (G–I) in R1 SE and R1 SE Jaw1 IE cells (A and G), R2 SE and R2 SE Jaw1 IE cells (B and H), and R3 SE and R3 SE Jaw1 IE cells (C and I). The averages of four wells are plotted in the graphs. (D–F and J–L) Mean curves (0–15 s) are enlarged from (A), (B), (C), (G), (H), and (I), respectively. Closed triangles represent the time points that ATP solution was added.

the generation of higher local Ca^{2+} concentration and promote the cycles of Ca^{2+} puff occurrence and Ca^{2+} diffusion in the cells, leading to the acceleration of the reaction speed in the cells expressing ITPR1 compared to other subtypes. Furthermore, the Ca^{2+} puff-occurred sites, thus ITPRs cluster, are distributed less tightly in the cells exclusively expressing ITPR1 than ITPR2 and ITPR3¹⁸. This factor also possibly contributes to the

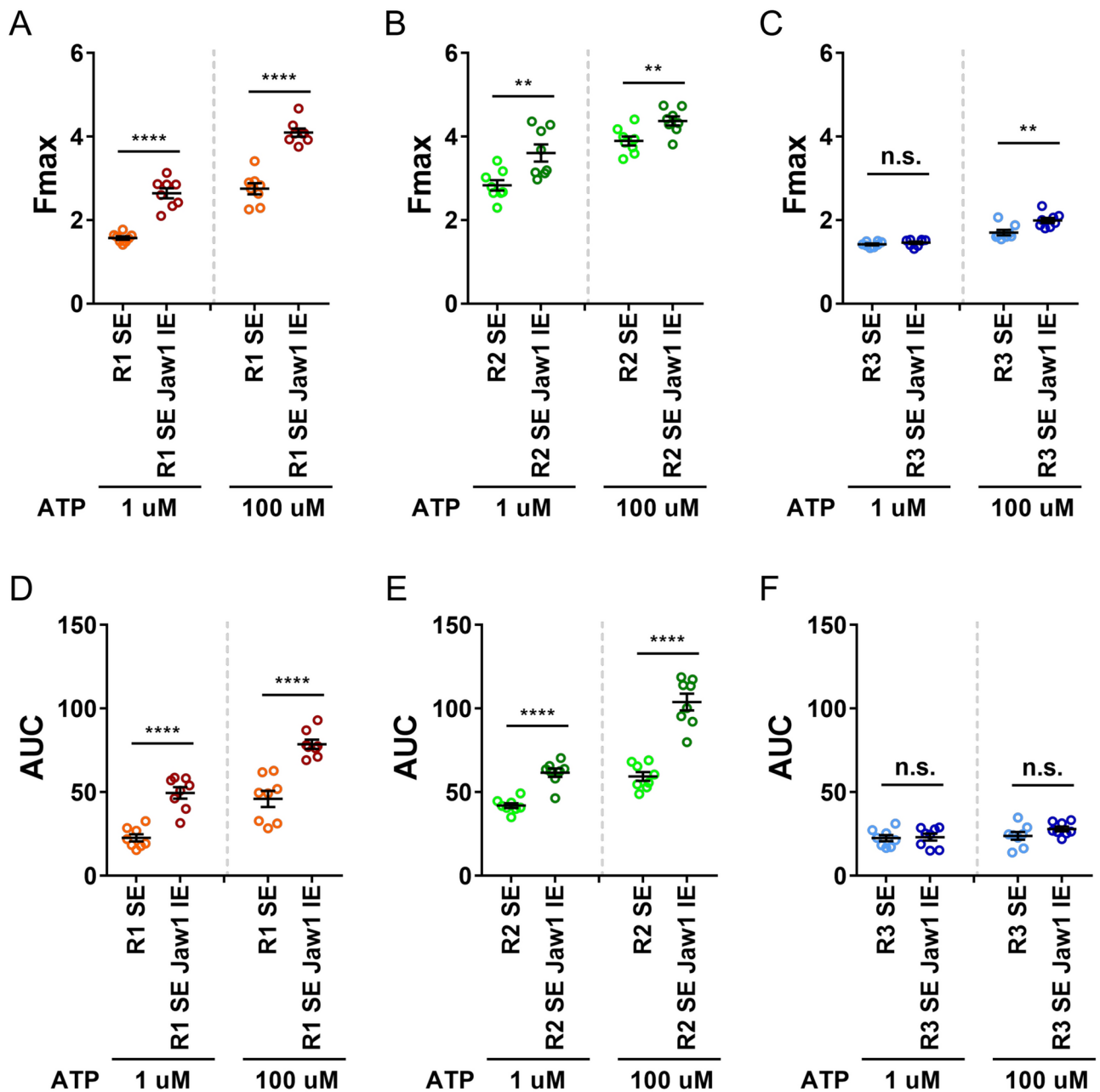


Fig. 4. Jaw1 increases the maximum amplitude and AUC of the Ca^{2+} signals in the cells expressing all ITPR subtypes. (A–C) F_{max} calculated from the plots in (A and G), (B and H), and (C and I) of Fig. 3, respectively. (D–F) AUC calculated from the plots in (A and G), (B and H), and (C and I) of Fig. 3, respectively. The averages of two independent experiments per condition ($n=4$) are shown in the graphs. In total, $n=8$. The error bar shows \pm S.D.; n.s., not significant; **, $p < 0.001$; ****, $p < 0.0001$; statistical analysis, two-tailed Student's t -test.

enhancement of the cycles of Ca^{2+} puff occurrence and Ca^{2+} diffusion in entire cells expressing ITPR1 rather than ITPR2 and ITPR3 under conditions of Jaw1 expression. The combination of ITPRs regulators including Jaw1 and ITPRs properties such as IP_3 sensitivity, Ca^{2+} concentration dependence, cluster distribution, etc. ultimately determines the reaction speed of the Ca^{2+} signal for each ITPR subtype in the cell. In addition to the above light microscopic analysis, structural approaches using a cryo-electron microscope will provide clues to identify the amino acid residues responsible for their interaction and regulation of ITPRs, which promotes understanding at the molecular level how Jaw1 regulates the Ca^{2+} signal via ITPRs with heterogeneous effects.

The mean differences in $\Delta T_{stimulation-F1.2}$ and $\Delta T_{stimulation-Fmax}$ between Jaw1 KO and Jaw1 IE cells were much more distinguished at lower concentrations of ATP, in contrast to that in AUC, as shown in Fig. 2H–J. The stimulation at higher concentrations of ATP promotes more IP_3 generation, activates more ITPRs, and elevates cytoplasmic Ca^{2+} concentrations more during a certain period, resulting in a shorter reaction speed of the Ca^{2+}

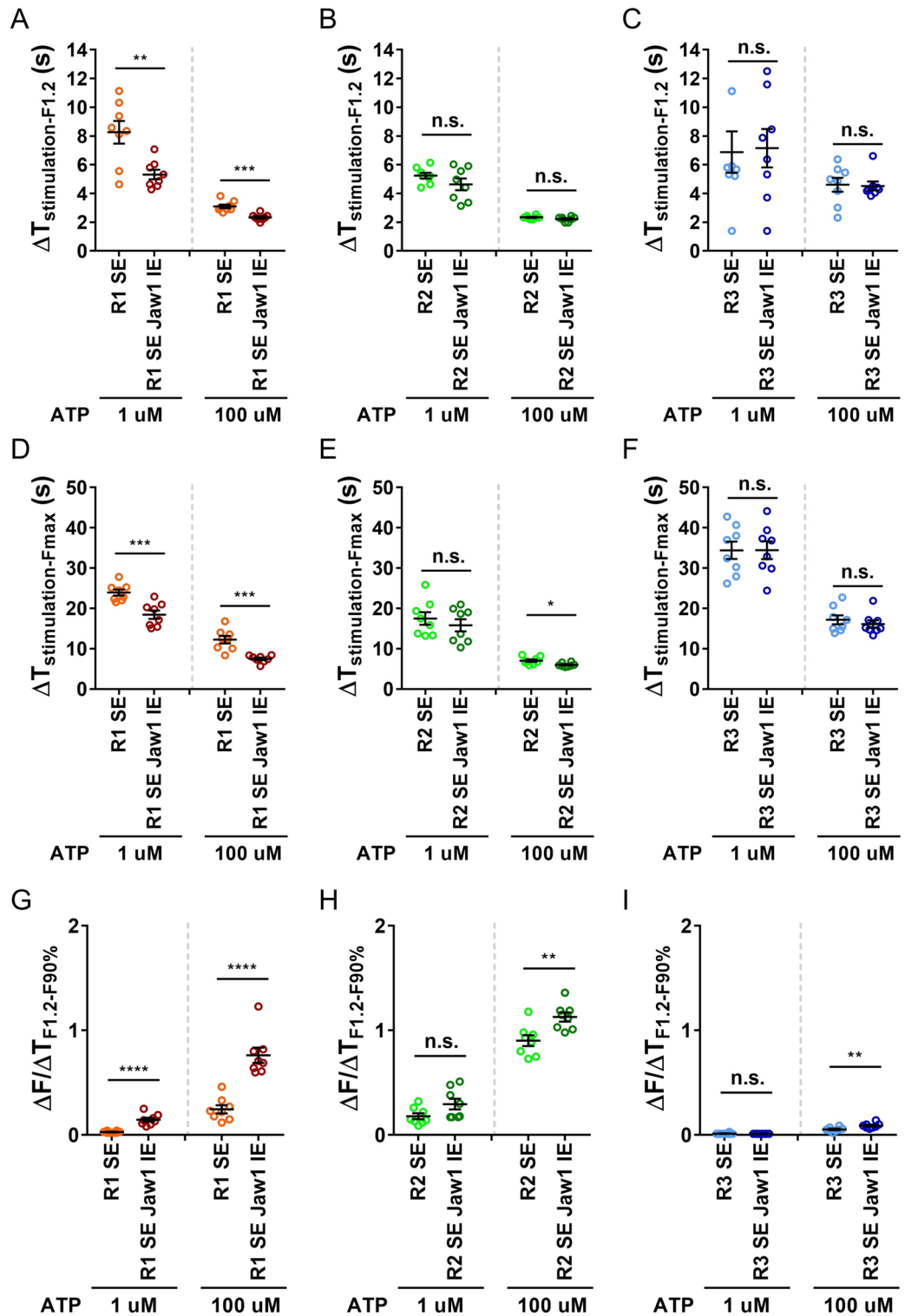


Fig. 5. Jaw1 accelerates the reaction speed of the Ca²⁺ signals upon GPCR stimulation in the cells expressing ITPR1. (A–C) $\Delta T_{\text{stimulation-F1.2}}$ calculated from the plots in (A and G), (B and H), and (C and I) of Fig. 3, respectively. (D–F) $\Delta T_{\text{stimulation-Fmax}}$ calculated from the plots in (A and G), (B and H), and (C and I) of Fig. 3, respectively. (G–I) $\Delta F/\Delta T_{F1.2-F90\%}$ calculated from the plots in (A and G), (B and H), and (C and I) of Fig. 3, respectively. The averages of two independent experiments per condition (n=4) are shown in the graphs. In total, n=8. The error bar shows \pm S.D.; n.s., not significant; *, $p < 0.05$; **, $p < 0.01$; ***, $p < 0.001$; ****, $p < 0.0001$; statistical analysis, two-tailed Student's *t*-test.

signals. However, the impacts on the reaction speed ultimately approach the saturation even under the state of the cells with augmentative effect by Jaw1, when the cells are stimulated at higher concentrations of ATP. It is probably due to the amount limitation of the activation for ITPRs per one cell during a single Ca^{2+} peak. In contrast, AUC is the total score of the accumulated Ca^{2+} peaks during the assay. The Ca^{2+} peaks occurred more frequently, thus oscillation, when the cells are stimulated with higher concentrations of ATP. Furthermore, the strength of each Ca^{2+} peak and oscillation are enhanced by Jaw1¹³. Therefore, the difference in AUC between Jaw1 KO and Jaw1 IE cells was much more distinguished at higher concentrations of ATP.

The time scale of Ca^{2+} signal-related physiological responses is different: exocytosis (μs), contraction (ms), metabolism (s), transcription (min), and fertilization and proliferation (h)⁶. The mean differences in the $\Delta T_{\text{stimulation-Fmax}}$ between Jaw1 KO and Jaw1 IE cells were on the level of seconds (on average: 1 μM ATP, 6.04 s; 10 μM ATP, 2.13 s; 100 μM ATP, 1.50 s) as shown in Fig. 2J. Those between R1 SE and R1 SE Jaw1 IE cells were also on the level of seconds scale (on average: 1 μM ATP, 5.49 s; 100 μM ATP, 4.76 s) as shown in Fig. 5D. Thus, the accelerating effect of Jaw1 on the reaction speed of the Ca^{2+} signals might be critical for physiological systems operating on a time scale of seconds. As a limitation in this study, we evaluated the reaction speed of Ca^{2+} signals using HEK293 cell lines as models, however, it was not tested whether those trends are the same as in any other cell types, especially under physiological conditions. The patterns of the Ca^{2+} curve upon GPCR stimulation vary depending on the involved ligands, receptors, other signaling-related molecules, cell types, etc., and the complicated combination of many factors including the expression fashions of ITPR subtypes and their regulators ultimately shape the patterns of Ca^{2+} curve^{1,11–14}. To date, the specific expression of Jaw1 has been identified in the taste cells on the tongue, small intestinal tuft cells, pancreatic acinar cells, and immune cells^{21,28–30}. Furthermore, the expression fashions of ITPR subtypes differ among these cell types: ITPR3 in taste cells, ITPR2 in tuft cells, and all subtypes in acinar cells. Although the reaction speed of the Ca^{2+} signals upon stimulation with carbachol seems to be delayed in the acinar cells lacking Jaw1 compared to wildtype, it remains unknown how the accelerating effect regulates the physiological function of acinar cells²⁹. It is therefore necessary to further explore the cell types or tissues where ITPR1 and Jaw1 co-express under physiological conditions. Additionally, further research should investigate how the relationship between the expression of Jaw1 and the regulation of Ca^{2+} dynamics, particularly in terms of reaction speed, contributes to physiological systems.

Materials and methods

Cell culture

All the cell lines used in this study were derived from HEK293 Flp-In T-REX cells (Thermo Fisher Scientific, #R78007), established and validated as previously described¹³. The cells were cultured in DMEM (Nacalai Tesque, #16919-42) supplemented with 10% fetal bovine serum (SIGMA-Aldrich, #F7524), 5.84 mg/mL L-glutamine (Nacalai Tesque, #16919-42), 100 U/mL penicillin, and 100 $\mu\text{g}/\text{mL}$ streptomycin (SIGMA-Aldrich, #P4333). Cells were grown in 5% CO_2 at 37 °C.

Calcium assay

Calcium assay was performed as previously described with some modifications¹³. In brief, each cell line was plated onto 96-well black wall plates (Greiner Bio-One, #655090). After overnight incubation, the expression of Jaw1 was induced by treatment with 200 ng/mL Dox for 24 h. The cells were washed with PBS once, and incubated with recording buffer (20 mM HEPES, pH 7.4, 115 mM NaCl, 5.4 mM KCl, 1.8 mM CaCl_2 , 0.8 mM MgCl_2 , 13.8 mM D-Glucose , and 1.25 mM probenecid) containing 2 μM Fluo-4 AM (dojindo, #F311) for 30 min. After washing the cells with recording buffer, the cells were incubated with recording buffer for 30 min. The well-scanning calcium assay was then performed using a plate reader, Varioskan LUX (Thermo Fisher Scientific). The fluorescence values were recorded every 0.11–0.13 s, and ATP (ORIENTAL YEAST Co., LTD., #45142000) diluted with recording buffer was added over 0.30 s at the time of the 11th recording. The fluorescence intensity at 0 s was defined as F0 and the relative fluorescence intensity at each time point was calculated as F/F0. The relative fluorescence intensity at each time point was then plotted to generate the Ca^{2+} curve. As shown in Fig. 1, F1.2, F90%, and Fmax were defined as the relative fluorescence intensity of which the scores first rise to 1.2, 90% of maximum amplitude, and maximum amplitude, respectively. $T_{\text{stimulation}}$ was defined as the time point at which ATP was added. $T_{\text{F1.2}}$, $T_{\text{F90\%}}$, and T_{Fmax} were defined as the time point at which the relative fluorescence intensity first rises to F1.2, F90%, and Fmax, respectively. $T_{\text{F1.2}}$ and T_{Fmax} were subtracted by $T_{\text{stimulation}}$, resulting in $\Delta T_{\text{stimulation-F1.2}}$ and $\Delta T_{\text{stimulation-Fmax}}$, which were defined as the scores for the signal onset time and rise time to the first peak top, respectively. F90% and $T_{\text{F90\%}}$ were subtracted by F1.2 and $T_{\text{F1.2}}$, resulting in ΔF and $\Delta T_{\text{F1.2-F90\%}}$, respectively. ΔF was then divided by $\Delta T_{\text{F1.2-F90\%}}$, resulting in $\Delta F/\Delta T_{\text{F1.2-F90\%}}$, which was defined as the score for the rise rate. The total increase of the relative fluorescence intensity during the assay (0–100 s) was calculated as AUC. The calculated data were then graphed in GraphPad Prism 7.

Statistical analysis

All statistical tests were calculated using GraphPad Prism 7, and the data were represented as the mean \pm S.D. An unpaired, nonparametric Student's *t*-test was used to compare two sample groups. *, **, ***, and **** indicate statistically significant *P*-values of $p < 0.05$, < 0.01 , < 0.001 , and < 0.0001 , respectively. n.s.: not significant.

Data availability

The datasets generated during and/or analyzed during the current study are available from the corresponding author upon reasonable request.

Received: 19 October 2024; Accepted: 13 March 2025

Published online: 24 March 2025

References

- Berridge, M. J., Lipp, P. & Bootman, M. D. The versatility and universality of calcium signalling. *Nat. Rev. Mol. Cell Biol.* **1**, 11–21 (2000).
- Bootman, M. D. & Bultynck, G. Fundamentals of cellular calcium signaling: a primer. *Cold Spring Harb. Perspect. Biol.* **12**, a038802 (2020).
- Berridge, M. J. Inositol trisphosphate and calcium signalling mechanisms. *Biochim. Biophys. Acta* **1793**, 933–940 (2009).
- Dhyani, V. et al. GPCR mediated control of calcium dynamics: a systems perspective. *Cell. Signal.* **74**, 109717 (2020).
- Marchant, J. S. & Parker, I. Functional interactions in Ca²⁺ signaling over different time and distance scales. *J. Gen. Physiol.* **116**, 691–696 (2000).
- Berridge, M. J., Bootman, M. D. & Roderick, H. L. Calcium signalling: dynamics, homeostasis and remodelling. *Nat. Rev. Mol. Cell Biol.* **4**, 517–529 (2003).
- Miyawaki, A. et al. Fluorescent indicators for Ca²⁺ based on green fluorescent proteins and calmodulin. *Nature* **388**, 882–887 (1997).
- Smith, I. F. & Parker, I. Imaging the quantal substructure of single IP₃R channel activity during Ca²⁺ puffs in intact mammalian cells. *Proc. Natl. Acad. Sci. U. S. A.* **106**, 6404–6409 (2009).
- Lock, J. T., Parker, I. & Smith, I. F. A comparison of fluorescent Ca²⁺ indicators for imaging local Ca²⁺ signals in cultured cells. *Cell Calcium* **58**, 638–648 (2015).
- Zhang, Y. et al. Fast and sensitive GCaMP calcium indicators for imaging neural populations. *Nature* **615**, 884–891 (2023).
- Ishida, S., Matsu-Ura, T., Fukami, K., Michikawa, T. & Mikoshiba, K. Phospholipase C-β1 and β4 contribute to non-genetic cell-to-cell variability in histamine-induced calcium signals in HeLa cells. *PLoS One* **9**, e86410 (2014).
- Emrich, S. M. et al. Omnitemporal choreographies of all five STIM/Orai and IP₃Rs underlie the complexity of mammalian Ca²⁺ signaling. *Cell Rep.* **34**, 108760 (2021).
- Okumura, W. et al. Jaw1/LRMP increases Ca²⁺ influx upon GPCR stimulation with heterogeneous effect on the activity of each ITPR subtype. *Sci. Rep.* **12**, 9476 (2022).
- Mikolajewicz, N., Smith, D., Komarova, S. V. & Khadra, A. High-affinity P2Y2 and low-affinity P2X7 receptor interaction modulates ATP-mediated calcium signaling in murine osteoblasts. *PLoS Comput. Biol.* **17**, e1008872 (2021).
- Prole, D. L. & Taylor, C. W. Inositol 1,4,5-trisphosphate receptors and their protein partners as signalling hubs. *J. Physiol.* **594**, 2849–2866 (2016).
- Miyakawa, T. et al. Encoding of Ca²⁺ signals by differential expression of IP₃ receptor subtypes. *EMBO J.* **18**, 1303–1308 (1999).
- Iwai, M., Michikawa, T., Bosanac, I., Ikura, M. & Mikoshiba, K. Molecular basis of the isoform-specific ligand-binding affinity of inositol 1,4,5-trisphosphate receptors. *J. Biol. Chem.* **282**, 12755–12764 (2007).
- Lock, J. T., Alzayady, K. J., Yule, D. I. & Parker, I. All three IP₃ receptor isoforms generate Ca²⁺ puffs that display similar characteristics. *Sci. Signal.* **11**, eaau0344 (2018).
- Kozono, T. et al. Jaw1/LRMP has a role in maintaining nuclear shape via interaction with SUN proteins. *J. Biochem.* **164**, 303–311 (2018).
- Okumura, W. et al. Jaw1/LRMP is associated with the maintenance of Golgi ribbon structure. *J. Biochem.* **173**, 383–392 (2023).
- Chang, C. Y. et al. Tumor suppressor p53 regulates intestinal type 2 immunity. *Nat. Commun.* **12**, 3371 (2021).
- Kozono, T. et al. Cleavage of the Jaw1 C-terminal region enhances its augmentative effect on the Ca²⁺ release via IP₃ receptors. *J. Cell Sci.* **136**, jcs260439 (2023).
- Bootman, M. D. & Berridge, M. J. Subcellular Ca²⁺ signals underlying waves and graded responses in HeLa cells. *Curr. Biol.* **6**, 855–865 (1996).
- Callamaras, N., Marchant, J. S., Sun, X. P. & Parker, I. Activation and co-ordination of InsP₃-mediated elementary Ca²⁺ events during global Ca²⁺ signals in *Xenopus* oocytes. *J. Physiol.* **509**, 81–91 (1998).
- Berridge, M. Elementary and global aspects of calcium signalling. *J. Physiol.* **499**, 291–306 (1997).
- Bezprozvanny, I., Watras, J. & Ehrlich, B. E. Bell-shaped calcium-response curves of Ins(1,4,5)P₃- and calcium-gated channels from endoplasmic reticulum of cerebellum. *Nature* **351**, 751–754 (1991).
- Kozono, T. et al. The N-terminal region of Jaw1 has a role to inhibit the formation of organized smooth endoplasmic reticulum as an intrinsically disordered region. *Sci. Rep.* **11**, 753 (2021).
- Behrens, T. W. et al. Jaw1, a lymphoid-restricted membrane protein localized to the endoplasmic reticulum. *J. Immunol.* **153**, 682–690 (1994).
- Prüschken, S., Majer, M., Schreiber, R. & Schlossmann, J. IRAG2 interacts with IP₃-receptor types 1, 2, and 3 and regulates intracellular Ca²⁺ in murine pancreatic acinar cells. *Int. J. Mol. Sci.* **22**, 13409 (2021).
- Shindo, Y. et al. Lrmp/Jaw1 is expressed in sweet, bitter, and umami receptor-expressing cells. *Chem. Senses* **35**, 171–177 (2010).

Acknowledgements

We thank Dr. Wataru Okumura and Mr. Hiroyuki Sato from Tokyo University of Agriculture and Technology for establishing the cell lines and technical supports. This work was supported by Grants-in-aid for Scientific Research from the Japan Society for Promotion of Science [23K14511 to T.K., 24K08698 to T.T.], and the Program on Open Innovation Platform with Enterprises, Research Institute and Academia (OPERA) from Japan Science and Technology Agency (JST) [JPMJOP1833 to A.N.].

Author contributions

Takuma Kozono: Conceptualization, Formal analysis, Writing—original draft, Visualization, Funding acquisition. Hitomi Matsui: Methodology, Validation, Investigation, Marielle Fernandez Bandalan: Writing—review & editing. Takashi Tonozuka: Writing—review & editing, Supervision, Funding acquisition. Atsushi Nishikawa: Conceptualization, Writing—review & editing, Supervision, Project administration, Funding acquisition.

Competing interests

The authors declare no competing interests.

Additional information

Correspondence and requests for materials should be addressed to A.N.

Reprints and permissions information is available at www.nature.com/reprints.

Publisher's note Springer Nature remains neutral with regard to jurisdictional claims in published maps and institutional affiliations.

Open Access This article is licensed under a Creative Commons Attribution-NonCommercial-NoDerivatives 4.0 International License, which permits any non-commercial use, sharing, distribution and reproduction in any medium or format, as long as you give appropriate credit to the original author(s) and the source, provide a link to the Creative Commons licence, and indicate if you modified the licensed material. You do not have permission under this licence to share adapted material derived from this article or parts of it. The images or other third party material in this article are included in the article's Creative Commons licence, unless indicated otherwise in a credit line to the material. If material is not included in the article's Creative Commons licence and your intended use is not permitted by statutory regulation or exceeds the permitted use, you will need to obtain permission directly from the copyright holder. To view a copy of this licence, visit <http://creativecommons.org/licenses/by-nc-nd/4.0/>.

© The Author(s) 2025